Disorder engineering: From structural coloration to acoustic filters

Nitin Upadhyaya[1,2] and Ariel Amir[1]
[1]*School of Engineering and Applied Sciences, Harvard University, Cambridge, Massachusetts 02138, USA*
[2]*Center for Mathematical Modeling, Flame University, Pune, Maharashtra 412115, India*

(Received 29 January 2018; published 5 July 2018)

We study localization of waves in a one-dimensional disordered metamaterial of bilayers composed of thin fixed length scatterers placed randomly along a homogenous medium. As an interplay between order and disorder, we identify a new regime of strong disorder where the localization length becomes independent of the amount of disorder but depends on the frequency of the wave excitation and on the properties of the fixed length scatterer. As an example of a naturally occurring nearly one-dimensional disordered bilayer, we calculate the wavelength-dependent reflection spectrum for Koi fish using the experimentally measured parameters and find that the main mechanisms for the emergence of their silver structural coloration can be explained through the phenomenon of localization of light in the regime of strong disorder discussed above. Finally, we show that, by tuning the thickness of the fixed length scatterer, the above design principles could be used to engineer disordered metamaterials which selectively allow harmonics of a fundamental frequency to be transmitted in an effect which is similar to the insertion of a half-wave cavity in a quarter-wavelength stack. However, in contrast to the Lorentzian resonant peak of a half-wave cavity, we find that our disordered layer has a Gaussian line shape whose width becomes narrower as the number of disordered layers is increased.

DOI: 10.1103/PhysRevMaterials.2.075201

I. INTRODUCTION

Metamaterials are composite materials engineered out of more commonly available materials by carefully arranging them in ways such that their collective response gives rise to novel mechanical and electromagnetic properties [1–9]. At the heart of any engineering design is the ability to accurately control the response of a system. Disorder thus seems manifestly at odds with the main principles of any engineering design. At the same time, random aggregates of objects, both natural [10,11] or man made [12–14], often display many novel properties which emerge in part from their intrinsic disorder. Yet, characterizing disorder and harnessing it to design materials whose response can be precisely controlled remains a challenge.

A periodic arrangement of a bilayer of materials consisting of regions of two different wave speeds (mechanical or electromagnetic) but with randomly varying thicknesses is a quintessential example of a one-dimensional disordered system whose transport properties are governed by wave localization [15–21]. Due to the mismatch in wave speeds at each interface of such a bilayer system, a part of the wave is reflected, and a part gets transmitted. Disorder in the path lengths in a sufficiently large sample can then eventually cause the reflected waves to interfere constructively in such a way that all the energy remains confined to a region of space, known as the localization length. The localization length in general depends upon both the nature and the amount of disorder and on the frequency of the incident wave. If the system length is much greater than the maximum localization length within the band of frequencies being considered, then wave transmission through the bilayer channel is effectively prevented, and, in the absence of any dissipative processes, all of the incident wave energy is reflected.

An intriguing prospect then is to ask the question: Could the disorder-induced localization length be harnessed to *design* metamaterials whose frequency response can be precisely controlled? Recent experiments have demonstrated how disorder-induced wave localization could be used to manipulate light on the nanoscale [22] and induce optical transitions from the spin-Hall effect in the regime of weak disorder to the random Rashba effect in the regime of strong disorder [23]. In this article, we study localization of waves in a one-dimensional disordered metamaterial consisting of thin fixed length scatterers placed randomly along a homogenous medium. We identify a different regime of wave localization whereby the localization length is independent of the amount of disorder (for sufficiently large disorder) yet depends only on the frequency of the wave excitation and on the properties of the fixed length scatterer. We use the transfer-matrix formulation to analytically derive the localization length and power transmission and compare these to corresponding results obtained numerically. As an example of a naturally occurring nearly one-dimensional disordered bilayer, we calculate the wavelength-dependent reflection spectrum for Koi fish using the experimental parameters discussed in Ref. [11] and find that the main mechanisms for the emergence of their silver structural coloration can be explained through the phenomenon of localization of light in the regime of strong disorder discussed above.

Finally, we use our results to propose the design of a simple one-dimensional mechanical metamaterial and discuss how, by tuning the wave speed and thickness of the scatterer, we can engineer disordered metamaterials which only allow the transmission of a narrow band of frequencies centered around the harmonics of the fundamental mode. We find that, in contrast to resonances in ordered systems, which typically have Lorentzian line shapes, here the transmission peak has a

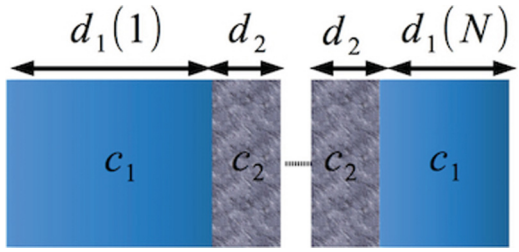

FIG. 1. A schematic of a periodic on average disordered metamaterial consisting of disordered bilayers of two materials with wave speeds c_1,c_2, respectively. The thickness of material 1, denoted by d_1, varies randomly whereas the thickness of material 2 is kept constant at a value of d_2 which is much smaller than the average value of d_1. This is reminiscent of the random Kronig-Penny model whereby we place scatterers (with thickness d_2 and wave speed c_2) randomly along the length of a homogenous background medium with wave speed c_1. For large variations in the thicknesses of material 1 (strong disorder), the localization length for a wave with frequency ω depends only on the properties of the scatterer as derived in Eq. (12). Thus, the parameters of material 2 can be tuned to design materials with a specific frequency response.

Gaussian shape with a width that decays as $1/\sqrt{N}$, where N is the number of layers, and thus can be made arbitrarily narrow. Thus, our paper adds to the growing interest in using disorder-induced wave localization to engineer novel properties.

II. WAVE LOCALIZATION IN A PERIODIC ON AVERAGE DISORDERED METAMATERIAL

Consider a homogenous medium with scatterers of fixed length placed randomly along a medium as in Fig. 1. This is reminiscent of the random Kronig-Penney model [24,25] where there is disorder in the thicknesses of only one of the layers (the background medium) comprising the bilayer whereas the thickness of the other is held constant at a value which is much smaller than the average thickness of the disordered layer.

In the following, we make use of the transfer-matrix formulation to study the reflectance and transmittance of a wave (electromagnetic or acoustic) impinging on this one-dimensional structure at normal incidence, although the approach presented generalizes to arbitrary angles of incidence. The transfer matrix which relates the forward going (E^+) and backward going (E^-) complex wave amplitudes across a bilayer can be written in the form (see Appendix A for the derivation)

$$\begin{pmatrix} E^+_{\text{after bilayer}} \\ E^-_{\text{after bilayer}} \end{pmatrix} = \mathcal{M} \begin{pmatrix} E^+_{\text{before bilayer}} \\ E^-_{\text{before bilayer}} \end{pmatrix},$$

where

$$\mathcal{M} = \begin{pmatrix} A & B \\ B^* & A^* \end{pmatrix}, \tag{1}$$

and

$$A = \frac{1}{1-r^2}(e^{i(\delta_1+\delta_2)} - r^2 e^{i(\delta_1-\delta_2)}), \tag{2}$$

$$B = \frac{2ir}{1-r^2} e^{-i\delta_1} \sin\,\delta_2, \tag{3}$$

where * denotes complex conjugation and we have defined $r = |\frac{n_2-n_1}{n_2+n_1}|$ as the reflection coefficient for normal incidence at the interface between medium 1 and medium 2 with optical refractive indices n_1,n_2, respectively. Here, $\delta_{1,2} = \frac{2\pi}{\lambda} n_{1,2} d_{1,2}$ are the phases accumulated by a wave of wavelength λ as it propagates media 1 and 2 with thicknesses $d_{1,2}$, respectively, see Fig. 1.

We may rewrite the transfer-matrix Eq. (1) in the form $\mathcal{M} = \mathcal{M}_s \mathcal{M}_b$, where $\mathcal{M}_s$ is a completely deterministic transfer matrix associated with the fixed length scatterer, and $\mathcal{M}_b$ is a random transfer matrix associated with the background medium,

$$\mathcal{M} = \frac{1}{1-r^2} \begin{pmatrix} e^{i\delta_2} - r^2 e^{-i\delta_2} & -2ir\,\sin\,\delta_2 \\ 2ir\,\sin\,\delta_2 & e^{-i\delta_2} - r^2 e^{i\delta_2} \end{pmatrix} \begin{pmatrix} e^{i\delta_1} & 0 \\ 0 & e^{-i\delta_1} \end{pmatrix}.$$

Here, the entries in the second matrix ($\mathcal{M}_b$) contain only δ_1 which is a random variable and denotes the phase accumulated by the wave as it traverses the background medium, whereas the entries in the first matrix ($\mathcal{M}_s$) contain only δ_2 which is a constant phase change as the wave traverses the scatterer.

The transfer matrix across $N+1$ barriers then is recursively given by $\mathbf{M}_{N+1} = \mathcal{M}_s \mathcal{M}_b \mathbf{M}_N$ and assumes the form

$$\mathbf{M}_{N+1} = \begin{pmatrix} \frac{1}{\tau_1^*} & -\frac{\rho_1^*}{\tau_1^*} \\ -\frac{\rho_1}{\tau_1} & \frac{1}{\tau_1} \end{pmatrix} \begin{pmatrix} \frac{1}{\tau_N^*} & -\frac{\rho_N^*}{\tau_N^*} \\ -\frac{\rho_N}{\tau_N} & \frac{1}{\tau_N} \end{pmatrix}, \tag{4}$$

where, ρ,τ are complex numbers representing the wave amplitude reflected and transmitted respectively, see Eqs. (A10) and (A11). Thus, the power transmitted $T_{N+1} = \frac{1}{|\mathbf{M}_{N+1}[1,1]|^2}$ is

$$T_{N+1} = \frac{T_N T_1}{1 + R_N R_1 + 2\sqrt{R_n R_1}\cos(\phi)}, \tag{5}$$

where we have expressed the reflectance and transmittance amplitudes in terms of the power reflected R and transmitted T using the relations $\rho_1 = \sqrt{R_1} e^{i\phi_1}$, $\rho_N = \sqrt{R_N} e^{i\phi_N}$, $\tau_N = \sqrt{T_N} e^{i\lambda_N}$ and defined $\phi = \phi_N - \phi_1 - 2\lambda_N$ to encode the random phase accumulated over the N layers.

Energy conversation and time-reversal symmetry provide us with an additional constraint [26],

$$\frac{\rho_N}{\rho_N^*} = -\frac{\tau_N}{\tau_N^*}, \tag{6}$$

using which, $\lambda_N = \phi_N + \frac{\pi}{2}$ and therefore, ϕ assumes an even simpler form—

$$\phi = \pi + \phi_1 + \phi_N. \tag{7}$$

Equation (7) has a clearer physical interpretation—ϕ is a random variable obtained by summing the reflection phases of individual bilayers through which the wave passes. The reflection phase of a single bilayer is obtained as $\rho = \frac{B^*}{A^*}$, see Eq. (A10), and when δ_2 is kept fixed, the reflection phase is $2\delta_1$ up to a constant. For strong disorder, i.e., when the standard deviation in the values of spacing d between scatterers is very large compared with the wavelength, we would expect the phase $\delta_1 = 2\pi \frac{d}{\lambda}$ to become uniformly distributed within the interval $[-\pi,\pi)$. Adding a uniformly distributed phase to another phase characterized by any distribution would result in a uniformly distributed phase. Therefore in the strong disorder regime we expect ϕ to be uniformly distributed. As we will

see in the following sections, even for moderate values of disorder in the strong disorder limit which we use in our paper, the resultant distribution of ϕ tends to be uniform, a result which we will be able to further validate when we compare our analytical results with numerical data.

Next, we take the logarithm of Eq. (5) (which we shortly justify) and then ensemble average both sides of the resultant equation [15] to obtain

$$\langle \ln\, T_{N+1}\rangle = \langle \ln\, T_N\rangle + \langle \ln\, T_1\rangle - \langle \ln[a + b\, \cos(\phi)]\rangle, \quad (8)$$

where $a = 1 + R_N R_1$ and $b = 2\sqrt{R_n R_1}$. If we now use the condition that the probability distribution of ϕ is nearly uniform, the ensemble average of the last term in Eq. (8) vanishes as follows:

$$\begin{aligned}\langle \ln[a + b\, \cos(\phi)]\rangle &= \frac{1}{2\pi}\int_0^{2\pi} \ln(a + b\, \cos\, \phi) d\phi,\\ &= \ln\left(\frac{1}{2}(a + \sqrt{a^2 - b^2})\right),\\ &= \ln\left(\frac{1}{2}(1 + R_N R_1 + |1 - R_N R_1|)\right),\\ &= 0, \end{aligned} \quad (9)$$

where the last line follows since $|R_N R_1| \leqslant 1$.

We now see one of the main advantages of taking the logarithm (see also Appendix B for a further discussion) of Eq. (5) for we have reduced Eq. (5) into a simple recursion relation,

$$\langle \ln\, T_{N+1}\rangle = \langle \ln\, T_N\rangle + \langle \ln\, T_1\rangle,$$

whose solution is

$$\langle \ln\, T_N\rangle = N\langle \ln\, T_1\rangle.$$

Substituting T_1 evaluated from Eq. (1), we find that T_1 does not depend on the random variable δ_1 but only on the fixed phase constant δ_2 and hence is a deterministic quantity. The average of the logarithmic power transmitted through N bilayers is therefore,

$$\begin{aligned}\langle \ln\, T_N\rangle &= -N\, \ln\left|\frac{1}{1 - r^2}(e^{i\delta_2} - r^2 e^{-i\delta_2})\right|^2,\\ &= -N\, \ln\left(1 + \frac{4r^2}{(1 - r^2)^2}\sin^2\delta_2\right). \end{aligned} \quad (10)$$

We can now invert the relation Eq. (10) to obtain the expected power transmitted through N bilayers (see also Ref. [27]),

$$T_N \sim e^{-Nd/\zeta}, \quad (11)$$

where $d = \langle d_1\rangle + d_2$ is the mean thickness of a bilayer and we obtain ζ as the localization length,

$$\zeta = \frac{d}{\ln\left(1 + \frac{4r^2}{(1-r^2)^2}\sin^2\delta_2\right)}. \quad (12)$$

The resultant Eq. (11) can be expressed as $T_N \sim \frac{1}{\left(1+\frac{4r^2}{(1-r^2)^2}\sin^2\delta_2\right)^N}$ or in other words, this suggests the power transmitted through the disordered layer can be obtained by taking the product of power transmitted through N ordered bilayers, see Eq. (A12) for comparison. This is a remarkably simple result, and even though it may seem that the resultant transmittance is a result of incoherent transmission of waves, that is not the case. Using the results of Ref. [18] for *incoherent* waves, one finds a Lorentzian line shape whose width scales as $1/\sqrt{N}$. In turn, Eq. (11) gives a transmission peak which is *Gaussian* and whose width also happens to scale as $1/\sqrt{N}$. To appreciate this, consider Eqs. (11) and (12). Defining $\Delta \equiv \frac{2r}{(1-r^2)}\sin\,\delta_2$, the resulting transmission for a system with $N \gg 1$ layers and in the regions where $\Delta^2 \ll 1$ is well approximated by

$$T_N \approx e^{-N\,\ln(1+\Delta^2)} = \frac{1}{(1 + \Delta^2)^N} \approx e^{-N\Delta^2}. \quad (13)$$

Furthermore, we see from Eq. (12) that under our assumptions of strong disorder, the localization length ζ is independent of the amount of disorder. However, since $\delta_2 = \frac{\omega}{c_2}d_2$, the localization length depends on the frequency of the incident wave ω and on the parameters of the scatterer. In the next section, we first discuss the optical case and see how our result Eq. (12) allows us to explain the observed reflection spectrum for Koi fish and consequently the main mechanisms for their silver structural coloration. This is one example of how nature harnesses disorder to engineer broadband reflectance. In the subsequent section, we will see how the localization length in Eq. (12) provides us with a way to harness disorder and engineer the frequency response of an acoustic disordered metamaterial.

What if we also allow the thickness of the scatterer to vary randomly? In that case, δ_2 in Eq. (10) is no longer a deterministic variable. However, if we continue to make the assumption that δ_2 is uniformly distributed over $[0,2\pi)$ and express $2\,\sin^2(\delta_2) = 1 - \cos(2\delta_2)$, we can ensemble average Eq. (10) in the same way as Eq. (9) to obtain

$$\begin{aligned}\langle \ln\, T_1\rangle &= -\frac{1}{2\pi}\int_0^{2\pi} \ln\left(1 + \frac{2r^2}{(1 - r^2)^2} - \frac{2r^2\cos(2\delta_2)}{1 - r^2}\right)d\delta_2,\\ &= -\ln\left(\frac{1}{1 - r^2}\right). \end{aligned} \quad (14)$$

This is exactly the result obtained in Ref. [18] where the authors explain the mirrorlike appearance of a stack of transparencies as a result of Anderson localization of light propagating through a one-dimensional disordered medium composed of bilayers of air and plastic, both of whose thicknesses vary randomly. Note here, the localization length in Eq. (14) depends only on the bare reflection coefficient r and neither on the magnitude of disorder nor on the frequency of the incident wave. Consequently, such a metamaterial will reflect back all incident frequencies, and this is what gives a stack of transparent materials its characteristic mirrorlike appearance. In Appendix C, we re-derive our result Eq. (12) using the method suggested in Refs. [17,18] for the case when the thickness of one of the layers comprising the bilayer is held constant.

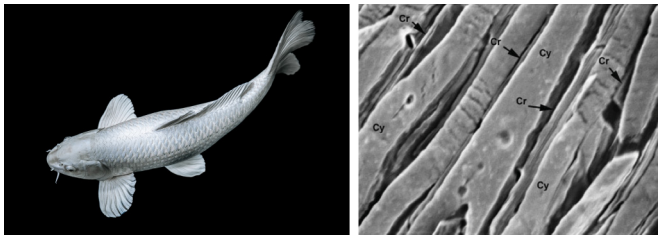

FIG. 2. *Left*: A butterfly Koi fish, exhibiting a broadband reflectance spectrum. *Right*: A magnified scanning electron microscopy (SEM) image of an iridophore cell extracted from the skin of Koi fish [11], well approximated as an alternating arrangement of guanine crystals (Cr) and cytoplasm (Cy). Image reproduced from Ref. [11], courtesy of Dr. D. Oron.

III. SILVER STRUCTURAL COLORATION IN FISH

The magnitude and distribution of ambient light is perhaps one of the most striking differences between terrestrial and oceanic life and has played a fundamental role in the evolution of the vertical segregation of habitats in our oceans [28]. In particular, the key factor determining camouflage in the mesopelagic realm (200–1000 m below sea level), essential for survival in the open ocean environments, is the uniformity of light distribution in all lateral directions. Under such conditions, a nearly transparent body structure (also found in upper ocean species and flowing rivers) or, more practically, a mirrorlike appearance that mimics transparency is most advantageous [28,29].

A mirrorlike appearance requires a broadband reflectance that reflects all wavelengths within the visible spectrum of light. Sea organisms, such as fish achieve this by covering their surface with millions of nearly one-dimensional micron-sized stacks, composed of a high refractive index material interspersed with a low refractive index material. Such a one-dimensional stack of bilayers is the most basic unit for structural colors in nature [30,31]. The basic optical structure in fish scales is well approximated by a one-dimensional stack of a crystalline organic substance—guanine with a refractive index of approximately $n_g \approx 1.83$, interspersed with layers of watery cytoplasm with a refractive index of approximately $n_c \approx 1.36$, see Fig. 2 (bottom) for a SEM image showing the one-dimensional optical stack in Koi fish. The disorder in these structures is manifest in the randomly varying thicknesses of either or both of these materials. As discussed in Refs. [32,33], wave localization provides a natural framework to study the reflection spectra of these disordered stacks.

The guanine-cytoplasm stack in Koi fish consists of cytoplasm layers whose thicknesses are normally distributed with a mean $d_c = 230$ nm and standard deviation $\sigma_c = 94$ nm, whereas the guanine layers are also normally distributed with a mean $d_g = 19$ nm and variation of $\sigma_g = 5$ nm [11]. Consequently, we will make the working assumption that the guanine-cytoplasm stack in Koi fish may be well approximated by a one-dimensional system of scatterers (guanine) placed randomly in a medium of cytoplasm implying that the transmission spectrum is well approximated by Eq. (11) with a localization length given in Eq. (12).

For comparison, we also discuss the case of Ribbon fish, which is another fish that displays silver coloration. The guanine-cytoplasm stack in Ribbon fish consists of cytoplasm layers whose thicknesses are uniformly distributed between 75 and 225 nm, whereas the thickness of the guanine layer is also uniformly distributed between 55 and 165 nm [10]. Defining the perturbation parameter $\epsilon = \frac{2\pi}{\lambda}\sigma$, we find that, for a typical $\lambda = 500$ nm and a standard deviation of $\sigma \approx 40$ nm, $\epsilon \approx 0.5$. As discussed and derived in Ref. [19], we can therefore consider this system weakly disordered, and by expanding the transfer matrices $\mathcal{M}_i$ to second order in ϵ, we obtain the localization length (note, the corresponding statistics for Koi fish is Gaussian with $\epsilon \approx 1.1$, and therefore the disorder regime for Koi is more appropriately classified as strongly disordered)—

$$l_r = (d_g + d_c)\left[\frac{\sin^2(\gamma\lambda)}{4\pi^2\left[n_g^2\sigma_g^2\sin^2(\delta_c) + n_c^2\sigma_c^2\sin^2(\delta_g)\right]\alpha^2}\right]. \tag{15}$$

Here, $n_{g,c}$ are the refractive indices for the guanine (g), cytoplasm (c) layers, $d_{c,g}$'s are their mean thicknesses, $\delta_{c,g} = \frac{2\pi}{\lambda}d_{c,g}$'s are the mean optical phases, whereas $\sigma_{g,c}$ are their respective standard deviations. As discussed in Sec. II, the bare reflection coefficient is defined as

$$r = \left|\frac{n_g - n_c}{n_g + n_c}\right|, \tag{16}$$

in terms of which, $\alpha = \frac{2r}{1-r^2}$, whereas γ is the mean complex Bloch wave vector, see Appendix A, Eq. (A13).

In Fig. 3, we have compared the numerically evaluated reflection spectrum (dotted curves) for normal incidence against the analytic expression (solid curves) given by

$$R = 1 - e^{-(2L/l_{r,k})}, \tag{17}$$

where L is the system size and $l_{r,k}$ are the localization lengths for the Ribbon fish (red curves) and for the Koi fish (blue curves), respectively, and find a reasonably good agreement over the visible spectrum. In Appendix D, we further study how the reflection spectrum of fish changes as we vary the thickness of the guanine layer (both the mean and its variance) which could help compare with other species of fish and future experimental data.

We stress that what we have considered is still a simplified model where the guanine-cytoplasm stack is assumed to be nearly one dimensional, and the effects of any spatial correlations are ignored. In the regime of strong disorder as defined in our paper, we do not anticipate spatial correlations to play any role since the localization length is independent of the amount of disorder, see Eq. (12). However, in the regime of weak disorder, Eq. (15) can be modified to incorporate correlations [19]. More accurate experimental data may reveal the actual regime to which the various fish parameters belong and in an ongoing work, we explicitly study the role of such spatial correlations in biological systems [34].

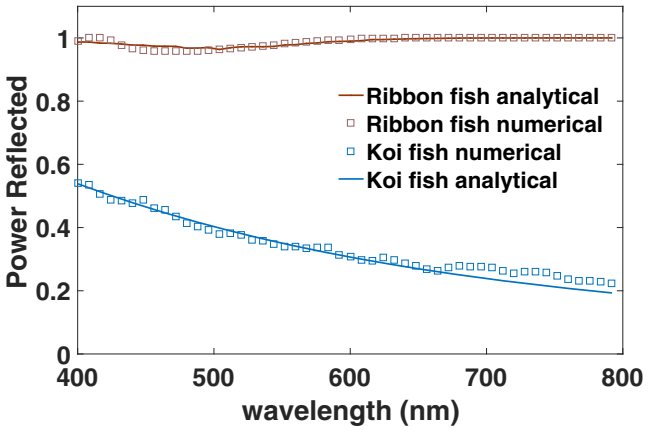

FIG. 3. The power reflected by a one-dimensional disordered stack of guanine crystals ($n_g = 1.83$) interspersed with layers of cytoplasm ($n_c = 1.36$). The blue curves correspond to parameters of the Koi fish with the thicknesses of cytoplasm layers Gaussian distributed between 230 nm and standard deviation 94 nm and the thickness of the guanine layer nearly constant at 19 nm for a total of 64 layers. For comparison, the red curves correspond to parameters of the Ribbon fish with thicknesses of cytoplasm layers uniformly distributed between 150 ± 75 nm and the thickness of the guanine layer uniformly distributed between 110 ± 55 nm for a total of 200 layers. Here, the square symbols are obtained numerically by ensemble averaging the logarithm of the transmitted power (T) over 1000 samples to evaluate the reflected power $1 - \exp(\langle \ln T \rangle)$, whereas the dashed curves are the analytical expression given in Eq. (17). The reflection spectrum corresponds to normal incidence.

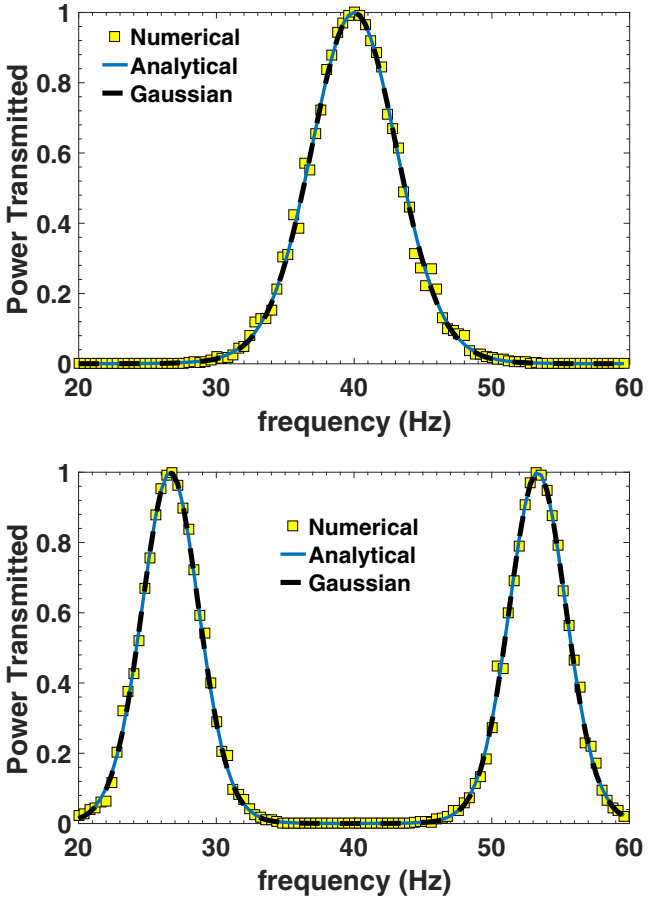

FIG. 4. The average power transmitted as a function of frequency through a disordered metamaterial consisting of a periodic on average alignment of 100 bilayers where the thickness of one of the layers (scatterer) is held constant at a value of d_2, whereas the thickness of the disordered layer is drawn from a uniform distribution between 0.1 and 0.9 m and we have chosen material sound speeds as $c_1 = 5.33$ and $c_2 = 4$ m/s and linear densities as $\rho_1 = 0.225$ and $\rho_2 = 0.4$ kg/m. As we change the thickness of the fixed length scatterer d_2, the channel allows the transmission of harmonics $f = \frac{n}{2}\frac{c_2}{d_2}$, where n is a positive integer. For illustration, we have chosen two values: $d_2 = 0.05$ m (top) and $d_2 = 0.075$ m (bottom). The symbols (yellow square) correspond to numerical data obtained after ensemble averaging 100 realizations of the logarithm of the power transmitted obtained by calculating the product of transfer matrices comprising the disordered metamaterial, the solid curve (blue) corresponds to the analytical expression derived in Eq. (11), whereas the dashed-dashed curve (black) corresponds to the Gaussian approximation given in Eq. (13).

IV. DESIGN OF NARROW PASSBAND DISORDERED ACOUSTIC METAMATERIALS

In the previous section, we discussed how wave localization could explain the main mechanisms of the origin of silver coloration in two species of fish. These constitute examples of natural occurring disordered systems where disorder has been harnessed to achieve broadband reflectance, important for the survival of many species of fish in their environment. In this section, we will discuss how the results in Eq. (11) can be used to open a narrow band of transmittance in an otherwise reflecting layer thereby utilizing disorder to design narrow passband transmittance filters. Since disorder-induced wave localization is a generic wave phenomena, we will discuss the design of narrow passband transmittance for the acoustic case. However, the same idea may be applied for the design of optical or microwave filters.

In Fig. 4, we compare the analytical results (dashed line) in Eq. (11) with the ensemble averaged power transmitted calculated numerically (square symbols) by evaluating the product of random transfer matrices comprising the disordered metamaterial. Here, the thickness of the disordered layer is drawn from a uniform distribution in the range of 0.1–0.9 m.

As we change the thickness of the fixed length scatterer d_2, the frequencies which are transmitted by the disordered metamaterial are the ones which make the localization length in Eq. (12) infinity and these occur when $\sin^2 \delta_2 = 0$, i.e., at frequencies of $f = \frac{n}{2}\frac{c_2}{d_2}$, where n is a positive integer, f is the frequency in hertz, and c_2 is the speed of sound through the scatterer. The plots shown in Fig. 4 correspond to $d_2 = 0.05$ m (top) and $d_2 = 0.075$ m (bottom). For instance, if $d_2 = 0.075$ m, $c_2 = 4$ m/s, the frequencies which are transmitted within the range of 20–60 Hz are $f_1 = n\frac{80}{3}$ for $n = 1,2$, i.e., harmonics of $f_0 = \frac{80}{3}$ Hz. As can be observed in Fig. 4, we have two peaks around $f_1 = 26.6$ Hz ($n = 1$) and around $f_2 = 53.3$ Hz ($n = 2$). All other frequencies within the range of 20–60 Hz are reflected. The material parameters chosen here or other values of sound speeds could, for instance, be realized using metamaterials with tunable elastic constants, such as a

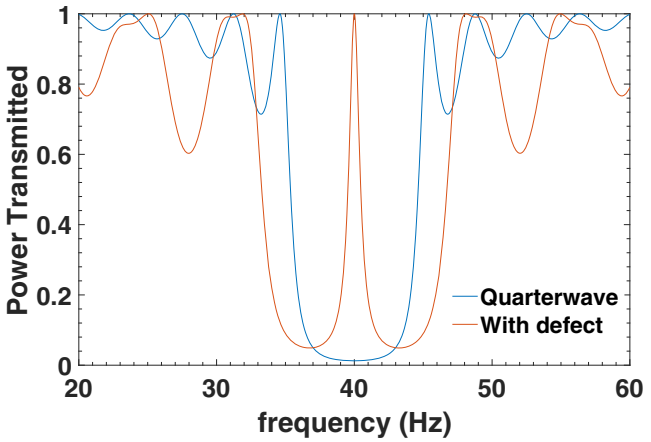

FIG. 5. The blue curve shows the power transmitted as a function of frequency through a periodic ordered bilayer (ten bilayers) channel formed from two materials with sound speeds $c_1 = 5.33$, $c_2 = 4.0$ m/s and with thicknesses tuned to quarter-wavelengths, whereas the red curve shows the power transmitted through a similar ordered bilayer (ten bilayers) after the introduction of a half-wavelength cavity tuned to give a transmittance peak near the center of the reflection band.

linear chain of elastic spheres [35] or quasi-one-dimensional spring networks [36].

Next, we compare the results of the disordered setup with those of an ordered system with a defect—effectively creating a cavity. Figure 5 shows the transmission spectrum of a purely ordered structure (blue curve) with layer thicknesses tuned to quarter-wavelengths creating a reflective layer centered around $f = 40$ Hz. This scenario can be solved exactly, and for completeness we derive the transmission of this setup in Appendix A. Upon insertion of a half-wave cavity in the otherwise quarter-wavelength reflecting stack [37,38], a narrow Lorentzian-shaped transmission peak is created [see Fig. 5 red curve] near the middle of the reflection band. One approach to analyze the transmission of this setup is to "lump" all the multilayers leading up to the defect into one element with reflection $\tilde{r}$ and transmittance $\tilde{t}$, which will also be the reflection and transmittance of the layers following the defect. Now the transmission coefficient is mathematically equivalent to that of a Fabry-Pérot setup and can readily be evaluated to give [26]

$$T \approx \frac{1}{1 + \frac{4R}{(1-R)^2}\sin^2(\delta_L)}, \tag{18}$$

with $R \equiv |\tilde{r}|^2$ and δ_L as the phase accumulated in the defect layer. For wavelengths within the stop bands of the ordered multilayer, $1 - R$ will be exponentially small in the number of layers, and we find

$$T \approx \frac{1}{1 + 4e^{N\Gamma}\sin^2(\delta_L)}, \tag{19}$$

with $\Gamma = i\gamma$ real and positive in the stop-band region, see Eq. (A13). The structure will thus show transmittance peaks when $n_L d = n\frac{\lambda}{2}$, i.e., at integer multiples of half-wavelengths. In contrast to Eq. (13), this has a Lorentzian form as is the typical case for resonances.

What, if any, are the design advantages of the disordered analog of the half-wave cavity? Even though the disordered design is not inherently superior to the ordered half-cavity effect in terms of performance, it has the advantage that it might be easier to fabricate since, if we have a way to synthesize layers of constant thickness, the Onsager mechanism of creating order based on entropic considerations alone could help self-organize a layered structure [39]. Such ordering may also arise due to flow as is the case in rheoscopic fluids [40].

To conclude, we have studied the localization of waves in a one-dimensional disordered metamaterial composed of fixed length scatterers placed randomly along a homogenous medium. As an interplay between order and disorder, we have identified a new regime of strong disorder where the localization length becomes independent of the amount of disorder but depends on the frequency of the wave excitation and on the properties of the fixed length scatterer. As an example of a naturally occurring disordered system, we have compared our analytical results with numerical results evaluated using experimentally obtained parameters for two species of fish and used the formalism of wave localization to explain the emergence of their silver structural coloration. Furthermore, we have discussed the design of a disordered narrow passband acoustic filter which gives a performance analogous to a half-wave cavity inserted in a quarter-wavelength reflecting stack. We believe our results could stimulate further analysis and experimental work harnessing disorder to engineer useful materials.

ACKNOWLEDGMENTS

We thank D. Oron, M. Kolle, C. Cook, K. Zhou, V. Manoharan, W. Rogers, and S. Joshi for useful discussions and the referees for their valuable feedback and suggestions for improvement. A.A. thanks the A.P. Sloan Foundation, the Kavli Foundation and the Harvard MRSEC Program of the NSF (DMR 14-20570) for their support.

APPENDIX A: REVIEW OF TRANSFER-MATRIX FORMULATION FOR AN ORDERED METAMATERIAL

Consider a dielectric bilayer composed of materials with refractive indices n_1,n_2 and thicknesses d_1,d_2, respectively, stacked along the z direction. The total electric field in any layer is a superposition of forward and reflected electric fields,

$$\tilde{E}_1 = E_1^+ e^{i\mathbf{k}_1\cdot\mathbf{r}} + E_1^- e^{i\mathbf{k}_1'\cdot\mathbf{r}}. \tag{A1}$$

Here, $E_1^{+,-}$ are the electric-field amplitudes where the superscripts $+,-$ denote forward and backward traveling waves, respectively, and $\mathbf{k}_1$,$\mathbf{k}_1'$ are the wave vectors specifying the direction of propagation of incident and reflected waves. Likewise, the total electric field in layer 2 is as follows:

$$\tilde{E}_2 = E_2^+ e^{i\mathbf{k}_2\cdot\mathbf{r}} + E_2^- e^{i\mathbf{k}_2'\cdot\mathbf{r}}. \tag{A2}$$

Next, assume that the incident wave makes an angle θ_1 with the normal to the interface situated at $z = d_1$. Then, from the boundary conditions, we obtain $|k_1| = |k_1'|$, $|k_1|\sin\theta_1 = |k_2|\sin\theta_2$, where θ_2 is the angle of refraction. For a plane-polarized wave we obtain the following constraints between

the electric-field amplitudes [41]:

$$\frac{1}{\alpha_1}E_1^+e^{i\delta_1}+\frac{1}{\alpha_1}E_1^-e^{-i\delta_1}=E_2^++E_2^-, \tag{A3}$$

$$\frac{1}{\beta_1}E_1^+e^{i\delta_1}-\frac{1}{\beta_1}E_1^-e^{-i\delta_1}=E_2^+-E_2^-, \tag{A4}$$

where $\mathbf{r}=d_1\hat{z}$ (along the direction of the stack) and we have defined $\delta_1=|k_1|d_1\cos\theta_1$. Here, $\alpha_1=\frac{\cos\theta_2}{\cos\theta_1}$ and $\beta_1=\frac{\mu_1 n_2}{\mu_2 n_1}$. It is convenient to express these relations in the form of a transfer matrix relating the electric-field amplitudes to the left and right of a dielectric layer—

$$\begin{pmatrix}E_2^+\\E_2^-\end{pmatrix}=\begin{pmatrix}\frac{\alpha_1+\beta_1}{2\alpha_1\beta_1}e^{i\delta_1} & \frac{\beta_1-\alpha_1}{2\alpha_1\beta_1}e^{-i\delta_1}\\ \frac{\beta_1-\alpha_1}{2\alpha_1\beta_1}e^{i\delta_1} & \frac{\alpha_1+\beta_1}{2\alpha_1\beta_1}e^{-i\delta_1}\end{pmatrix}\begin{pmatrix}E_1^+\\E_1^-\end{pmatrix}.$$

Note, due to energy conservation (we have assumed no absorption) and time-reversal invariance, the transfer matrix has a real trace and a unit determinant [42]. Consequently, any product of these matrices will also have a unit determinant.

Likewise, for the wave incident from medium 2 to medium 1, $\beta_2=\frac{1}{\beta_1}$, $\alpha_2=\frac{1}{\alpha_1}$, and $\delta_2=|k_2|d_2\cos\theta_2$, and we find the matrix relation,

$$\begin{pmatrix}E_3^+\\E_3^-\end{pmatrix}=\begin{pmatrix}\frac{\alpha_1+\beta_1}{2}e^{i\delta_2} & -\frac{\beta_1-\alpha_1}{2}e^{-i\delta_2}\\ -\frac{\beta_1-\alpha_1}{2}e^{i\delta_2} & \frac{\alpha_1+\beta_1}{2}e^{-i\delta_2}\end{pmatrix}\begin{pmatrix}E_2^+\\E_2^-\end{pmatrix}.$$

The overall transfer matrix for the bilayer is now

$$\mathcal{M}=\begin{pmatrix}A & B\\ B^* & A^*\end{pmatrix}, \tag{A5}$$

where

$$A=\frac{1}{1-r^2}(e^{i(\delta_1+\delta_2)}-r^2e^{i(\delta_1-\delta_2)}), \tag{A6}$$

$$B=\frac{2ir}{1-r^2}e^{-i\delta_1}\sin\delta_2, \tag{A7}$$

where $r=\frac{\beta_1-\alpha_1}{\beta_1+\alpha_1}$. (An identical calculation for a wave that is polarized perpendicular to the plane leads to the same form for the transfer matrix with the replacement $r=\frac{\alpha_1\beta_1-1}{\alpha_1\beta_1+1}$).

Next, we define the product of $N-1$ matrices as $\mathbf{M}_N=\mathcal{M}_{N-1}\mathcal{M}_{N-2}\cdots\mathcal{M}_1$ to obtain the overall relation between the incident wave amplitude and the wave amplitude after traversing N bilayers—

$$\begin{pmatrix}E_N^+\\E_N^-\end{pmatrix}=\mathbf{M}_N\begin{pmatrix}E_1^+\\E_1^-\end{pmatrix}. \tag{A8}$$

Upon normalizing the columns in Eq. (A8) with respect to the incident wave amplitude E_1^+, we find

$$\begin{pmatrix}\frac{E_N^+}{E_1^+}\\ \frac{E_N^-}{E_1^+}\end{pmatrix}=\mathbf{M}_N\begin{pmatrix}1\\ \frac{E_1^-}{E_1^+}\end{pmatrix}. \tag{A9}$$

By definition, the (complex) transmitted amplitude is $\tau=\frac{E_N^+}{E_1^+}$, and the complex reflection amplitude is $\rho=\frac{E_1^-}{E_1^+}$, whereas there is no backward propagating wave at the end of the N layers, i.e., $\frac{E_N^-}{E_1^+}=0$. Solving the matrix equations, we find

$$\tau=\mathbf{M}_N(1,1)+\mathbf{M}_N(1,2)\rho,$$

$$0=\mathbf{M}_N(2,1)+\mathbf{M}_N(2,2)\rho,$$

where, in addition, $\mathbf{M}_N^*(1,1)=\mathbf{M}_N^*(2,2)$ and $\mathbf{M}_N^*(1,2)=\mathbf{M}_N^*(2,1)$. Solving these, we obtain

$$\rho=-\frac{\mathbf{M}_N(2,1)}{\mathbf{M}_N(2,2)}, \tag{A10}$$

and

$$\tau=\frac{\mathbf{M}_N(2,2)\mathbf{M}_N(1,1)-\mathbf{M}_N(2,1)\mathbf{M}_N(1,2)}{\mathbf{M}_N(2,2)}.$$

Since $\det\{\mathbf{M}_N\}=1$, the above expression simplifies to

$$\tau=\frac{1}{\mathbf{M}_N(2,2)}. \tag{A11}$$

Therefore, the overall power transmitted is $|\tau|^2=T=\frac{1}{|\mathbf{M}_N[1,1]|^2}=\frac{1}{|\mathbf{M}_N[2,2]|^2}$. By energy conservation, the power reflected is $R=1-T$.

For the ordered case, where all the layers have the same thicknesses, we have the following analytic expression for the overall power transmitted [24]:

$$T_N=\frac{1}{1+|\mathcal{M}(1,2)|^2\left(\frac{\sin(N\gamma)}{\sin(\gamma)}\right)^2}, \tag{A12}$$

where γ is the complex Bloch wave vector that satisfies the condition,

$$2\cos\gamma=\mathrm{Tr}\{\mathcal{M}\}. \tag{A13}$$

An analogous derivation follows for one-dimensional mechanical displacement fields (acoustic) where we identify the parameter $\beta=\frac{\rho_2c_2}{\rho_1c_1}$ where $\rho_{1,2}$ are the densities of the two layers comprising the bilayer and $c_{1,2}$ is the corresponding speed of sound in the respective layers.

APPENDIX B: LOGARITHMIC AVERAGING

To intuitively appreciate the advantage of taking the logarithm of a product of random variables, consider the product of N-independent (positive) random variables—

$$S=x_1x_2x_3\cdots x_N. \tag{B1}$$

Under general assumptions where the central limit theorem holds, we would expect the sum of logarithms,

$$\ln(S)=\ln(x_1)+\ln(x_2)+\ln(x_3)\cdots\ln(x_N) \tag{B2}$$

to obey the central limit theorem. Consequently, $\ln(S)$ in Eq. (B2) will be normally distributed whose mean and mode coincide, whereas the distribution of S will be a lognormal. If the mean and mode coincide, then the most likely value of the random variable coincides with the average, which is a good feature. A generalized version of the central limit theorem for a product of 2×2 random matrices with entries which are complex numbers is given in Ref. [43].

Furthermore, for a disordered one-dimensional system, it can be shown that the ratio of variance of $\ln(S)$ in Eq. (B2) to its mean-squared value (relative fluctuations) decays linearly with the system size whereas for the variable S in Eq. (B1), the relative fluctuations grow exponentially with the system size, see Ref. [44] for a derivation of this result. Thus, the logarithm of the power transmittance has better self-averaging properties.

APPENDIX C: ALTERNATE DERIVATION OF LOCALIZATION LENGTH

In this appendix, we re-derive the localization length Eq. (12) by following the derivations in Ref. [18], albeit, keeping track of an additional wavelength-dependent factor which, in this case, comes from the barrier layer having a nearly constant thickness. Since the random variations occur in only the background medium, we write the transfer matrix given in Eq. (1) for the nth bilayer as

$$\mathcal{M}_n = \frac{|E|e^{-i\delta_n}}{1-r^2}\begin{pmatrix} \frac{E}{|E|}z_n & \frac{\Sigma}{|E|} \\ \frac{\Sigma^*}{|E|}z_n & \frac{E^*}{|E|} \end{pmatrix}, \\ = \frac{|E|e^{-i\delta_n}}{1-r^2}\tilde{\mathcal{M}}_n,$$

where $E = e^{i\delta_2} - r^2 e^{-i\delta_2}$, $\Sigma = 2ir\,\sin\,\delta_2$, and $z_n = e^{2i\delta_n}$. Here, δ_2 is a constant phase across the barrier layer (no random variation), whereas δ_n is the random phase accumulated as the wave propagates through the background layer after n bilayers.

For a stack of N bilayers, we use the following definition for the Lyapunov exponent (which is proportional to the inverse Anderson localization length):

$$\zeta_b = 2\lim_{N\to\infty}\frac{\mathrm{Re}\langle \ln\,\mathrm{Tr}\{\mathbf{M}_N\}\rangle}{N}, \tag{C1}$$

whereby we need to evaluate the expression,

$$\mathrm{Re}\left\langle \ln\left[\left(\frac{|E|}{1-r^2}\right)^N e^{-i(\delta_1+\delta_2\cdots+\delta_n)}\mathrm{Tr}\{\tilde{\mathcal{M}}_n\cdots\tilde{\mathcal{M}}_1\}\right]\right\rangle. \tag{C2}$$

Upon taking the real part of Eq. (C2), the exponential factor containing random phases drops out. The expectation value can now be evaluated by assuming that, due to strong disorder, the phases δ_n take all possible values from 0 to 2π. Thus, we convert the phase integral into a contour integral in terms of the complex random variable z_n (where $|z_n| = 1$ over the unit circle) to obtain the expression [18],

$$\zeta_b = 2\,\ln\left(\frac{|E|}{1-r^2}\right) + 2\lim_{N\to\infty}\frac{1}{(2\pi i)^N}\oint\frac{dz_1}{z_1}\cdots\oint\frac{dz_n}{z_n} \\ \times\,\ln\,\mathrm{Tr}\left[\begin{pmatrix} \frac{E}{|E|}z_1 & \frac{\Sigma}{|E|} \\ \frac{\Sigma^*}{|E|}z_1 & \frac{E^*}{|E|}\end{pmatrix}\cdots\begin{pmatrix} \frac{E}{|E|}z_n & \frac{\Sigma}{|E|} \\ \frac{\Sigma^*}{|E|}z_n & \frac{E^*}{|E|}\end{pmatrix}\right]. \tag{C3}$$

The contour integrals on the right-hand side are given by the residues at $z_k = 0$ ($k = 1\cdots n$) and therefore vanish [18]. Consequently, the exponent is

$$\zeta_b = \ln\left(1 + \frac{4r^2}{(1-r^2)^2}\sin^2(\delta_2)\right), \tag{C4}$$

from where the localization length in the strongly disordered regime is

$$l_b = \frac{d}{\zeta_b}, \tag{C5}$$

recovering Eq. (12) given in the main text.

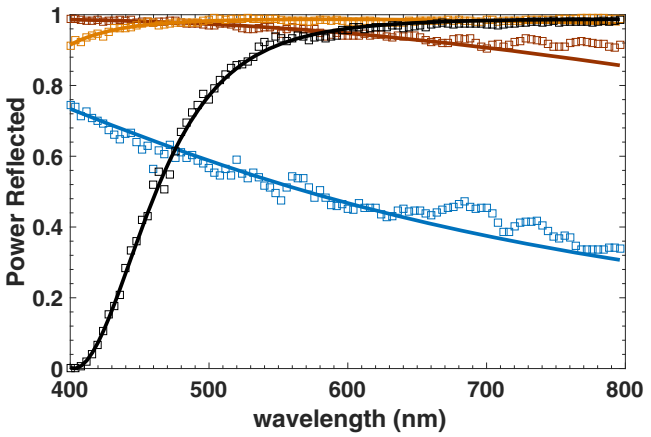

FIG. 6. We compare the spectrum of reflected power obtained analytically (solid curves) as given in Eq. (17) where the localization length is given in Eq. (12) with the numerical data obtained after ensemble averaging 100 realizations of the logarithm of the power transmitted obtained by calculating the product of transfer matrices comprising the disordered medium (square symbols). Here, the colors correspond to thicknesses of the guanine layers d_g = 19 nm (blue), d_g = 50 nm (maroon), d_g = 80 nm (orange), and d_g = 110 nm (black) with no random variations whereas the thickness of cytoplasm layer is drawn from a Gaussian distribution with mean d_c = 230 nm and standard deviation σ_c = 94 nm.

APPENDIX D: DEPENDENCE OF THE FISH REFLECTION SPECTRUM ON THE THICKNESS OF GUANINE-CYTOPLASM LAYERS

In this appendix, we study how the reflection spectrum of fish changes as we explore a subset of the guanine-cytoplasm thickness parameter space. To study the effects of the mean thickness of the guanine layer on the reflection spectrum of fish, we assume that the guanine layer has no disorder and vary its thickness from d_g = 19 nm (blue), d_g = 50 nm (maroon), d_g = 80 nm (orange) to d_g = 110 nm (black) as shown in Fig. 6. Furthermore, we assume that the statistics of the cytoplasm layer is drawn from a Gaussian distribution with mean d_c = 230 nm and standard deviation σ_c = 94 nm.

As we see in Fig. 6, the reflected power evaluated numerically (square symbols) compares very well with the reflected power evaluated analytically using Eq. (17) from the main text—

$$R \sim 1 - \exp(-L/\zeta), \tag{D1}$$

where L is the system size and ζ is the localization length, which for the guanine layer of constant thickness is given in Eq. (12) of the main text. Barring the change in intensity of the power reflected, we see that a broadband reflectance is obtained for d_g = 20,50,80 nm. However, when d_g = 110 nm (black curve), we find that a lower cutoff gets introduced in the visible spectrum at around λ = 400 nm and we expect that this cutoff will tend to make the appearance of fish silver, see Ref. [45] for plots of the reflection spectrum of metallic silver. Furthermore, we have checked that, in this regime of strong disorder, varying the mean thickness of the cytoplasm layers (from d_c = 150 to 240 nm) does not effect the reflection spectrum.

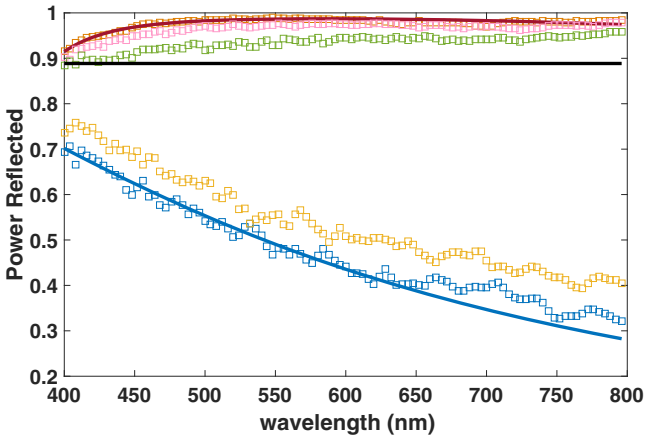

FIG. 7. Comparison of numerical (symbols) and analytical (solid) plots of the reflection spectrum with the statistics of the cytoplasm layer drawn from a Gaussian distribution with mean $d_c = 230$ nm and standard deviation $\sigma_c = 94$ nm whereas that of the guanine layer also drawn from a Gaussian distribution with two choices of mean: (1) $d_g = 80$ nm and standard deviation $\sigma_g = 0$ nm (orange square symbols), $\sigma_g = 20$ nm (pink square symbols), and $\sigma_g = 40$ nm (green square symbols) and (2) $d_g = 19$ nm and standard deviation $\sigma_g = 0$ nm (blue square symbols) and $\sigma_g = 10$ nm (yellow square symbols). Here, the horizontal black line corresponds to the wavelength- and disorder-independent reflection spectrum obtained using Eq. (D1) with $\zeta \sim \frac{-1}{\ln(1-r^2)}$ as derived in Eq. (14), the solid maroon curve corresponds to using Eq. (D1) with the localization length derived in Eq. (12) with the mean thickness of the guanine layer $d_g = 80$ nm, whereas the solid blue curve corresponds to using Eq. (D1) with the localization length derived in Eq. (12) with the mean thickness of the guanine layer $d_g = 19$ nm (the parameters of the Koi fish are discussed in the main text).

In Fig. 7, we explore how the reflection spectrum of fish changes if the thickness of the guanine layer also varies randomly. Here, we continue to assume that the thickness of the cytoplasm layer is drawn from a Gaussian distribution with mean $d_c = 230$ nm and standard deviation $\sigma_c = 94$ nm whereas that of the guanine layer is also drawn from a Gaussian distribution with two choices of the mean thickness and varying disorder: (1) $d_g = 80$ nm with standard deviation $\sigma_g = 0$ nm (orange square symbols), $\sigma_g = 20$ nm (pink square symbols), and $\sigma_g = 40$ nm (green square symbols) and (2) $d_g = 19$ nm with standard deviation $\sigma_g = 0$ nm (blue square symbols) and $\sigma_g = 10$ nm (yellow square symbols). Here, the horizontal black line corresponds to the wavelength- and disorder-independent reflection spectrum obtained using Eq. (D1) with localization length,

$$\zeta = -\frac{(d_g + d_c)}{\ln(1 - r^2)}, \tag{D2}$$

as derived in Eq. (14), whereas the blue and maroon curves correspond to the localization length derived in Eq. (12) with mean thicknesses of 19 and 80 nm, respectively.

As we see from Fig. 7, for zero or small values of disorder in the thickness of the guanine layer (blue, orange, and pink squares), the numerical data continue to agree reasonably well with the regime of localization derived in the text for Koi fish. However, for $d_g = 80$, $\sigma_g = 40$ nm (green square symbols), we find a crossover in the reflection spectrum with the localization length agreeing better with Eq. (D2) at lower wavelengths and with the weak disorder regime described by Eq. (15) at higher wavelengths (around 1500 nm and above, not shown in the figure).

Furthermore, when $d_g = 19$ and $\sigma_g = 10$ nm (yellow square symbols), i.e., the case of thin guanine layers discussed in the main text but with disorder added, we see that the reflection spectrum continues to follow the curve described by the wavelength-dependent localization length derived in Eq. (12) except that the intensity of the power reflected is higher. Note that, in the case of such thin layers, we do not see a crossover to a wavelength-independent reflection spectrum described by Eq. (14). In order to see such a crossover within the visible spectrum, the mean thickness of both layers comprising the bilayer should be greater than around 100 nm so that, in a disordered sample, the ratio of standard deviation to wavelengths is at least unity (strong disorder for both layers comprising the bilayer). Qualitatively however, we continue to expect a white-silver appearance for the fish within the parameter space explored in Fig. 7.

We further explore the effects of disorder and spatial correlations in biological systems in an ongoing work [34].

[1] N. Engheta and R. W. Ziolkowski, *Metamaterials: Physics and Engineering Explorations* (Wiley, Hoboken, NJ, 2006).
[2] *Acoustic Metamaterials and Phononic Crystals*, edited by P. A. Deymier, Springer Series in Solid-State Sciences Vol. 173 (Springer, Berlin/Heidelberg, 2013).
[3] W. Cai and V. Shalaev, *Optical Metamaterials: Fundamentals and Applications* (Springer, New York, 2009).
[4] J. B. Pendry and D. R. Smith, Reversing light: Negative refraction, Phys. Today **57**(6), 37 (2003).
[5] D. Schurig *et al.*, Metamaterial electromagnetic cloak at microwave frequencies, Science **314**, 977 (2006).
[6] A. Alu and N. Engheta, Guided modes in a waveguide filled with a pair of single-negative (SNG), double-negative (DNG), and/or double-positive (DPS) layers, IEEE Trans. Microwave Theory Tech. **52**, 199 (2004).
[7] K. Bertoldi, P. M. Reis, S. Willshaw, and T. Mullin, Negative poisson's ratio behavior induced by an elastic instability, Adv. Mater. **22**, 361 (2009).
[8] S. Zhang, C. Xia, and N. Fang, Broadband Acoustic Cloak for Ultrasound Waves, Phys. Rev. Lett. **106**, 024301 (2011).
[9] C. Q. Cook and A. Amir, Theory of chirped photonic crystals in biological broadband reflectors, Optica **3**, 1436 (2016).
[10] D. R. McKenzie, Y. Yin, and W. D. McFall, Silvery fish skin as an example of chaotic reflector, Proc. R. Soc. London, Ser. A **451**, 579 (1995).
[11] A. Levy-Lior *et al.*, Guanine based biogenic photonic crystal arrays in fish and spiders, Adv. Funct. Mater. **20**, 320 (2010).
[12] M. van Hecke, Jamming of soft particles: Geometry, mechanics, scaling and isostaticity, J. Phys.: Condens. Matter **22**, 033101 (2009).

[13] V. F. Nesterenko, *Dynamics of Heterogeneous Materials* (Springer-Verlag, New York, 2001).
[14] O. Brandt and K. H. Ploog, Solid-state lighting: The benefit of disorder, Nat. Mater. **5**, 769 (2006).
[15] P. W. Anderson, Absence of diffusion in certain random lattices, Phys. Rev. **109**, 1492 (1958).
[16] W. S. Diederik, B. Paolo, A. Lagendijk, and R. Righini, Localization of light in a disordered medium, Nature (London) **390**, 671 (1997).
[17] V. Baluni and J. Willemsen, Transmission of acoustic waves in a random layered medium, Phys. Rev. A **31**, 3358 (1985).
[18] M. V. Berry and S. Klein, Transparent mirrors: Rays, waves and localization, Eur. J. Phys. **18**, 222 (1997).
[19] F. M. Izrailev and N. M. Makarov, Localization in Correlated Bilayer Structures: From Photonic Crystals to Metamaterials and Semiconductor Superlattices, Phys. Rev. Lett. **102**, 203901 (2009).
[20] E. Abrahams, *50 years of Anderson Localization* (World Scientific, Singapore, 2010).
[21] *Optical Properties of Photonic Structures: Interplay of Order and Disorder*, edited by M. F. Limonov and M. Richard (CRC Press, Boca Raton, FL, 2012).
[22] Shi *et al.*, Strong localization of surface plasmon polaritons with engineered disorder, Nano Lett. **18**, 1896 (2018).
[23] E. Maguid *et al.*, Disorder-induced optical transition from spin Hall to random Rashba effect, Science **358**, 1411 (2017).
[24] G. A. Luna-Acosta, F. M. Izrailev, N. M. Makarov, U. Kuhl, and H. J. Stöckmann, One dimensional Kronig-Penney model with positional disorder: Theory versus experiment, Phys. Rev. B **80**, 115112 (2009).
[25] P. Markoš and C. M. Soukoulis, *Wave Propagation: From Electrons to Photonic Crystals and Left-Handed Materials* (Princeton University Press, Princeton, 2008).
[26] A. Amir and P. Vukusic, Elucidating the stop bands of structurally colored systems through recursion, Am. J. Phys. **81**, 253 (2013).
[27] Regarding the notation here, we are not implying that mean (T) is the same as exp[mean(ln T)], rather, Eq. (11) is simply to suggest that the value of transmission we expect to observe is exp[mean(ln T)].
[28] P. Herring, *The Biology of the Deep Ocean* (Oxford University Press, New York, 2002).
[29] E. J. Denton, On the organization of reflecting surfaces in some marine animals, Philos. Trans. R. Soc., B **258**, 285 (1970).
[30] Lord Rayleigh, On the reflection of light from a regularly stratified medium, Proc. R. Soc. London, Ser. A **93**, 565 (1917).
[31] S. Kinoshita, *Structural Colors in the Realm of Nature* (World Scientific, Singapore, 2008).
[32] T. M. Jordan, J. C. Partridge, and N. W. Roberts, Non-polarizing broadband multilayer reflectors in fish, Nat. Photon. **6**, 759 (2012).
[33] T. M. Jordan, J. C. Partridge, and N. W. Roberts, Disordered animal multilayer reflectors and the localization of light, J. R. Soc., Interface **11**, 20140948 (2014).
[34] K. Zhou and A. Amir, Theory and Design of Photonic Crystals in Broadband Biological Reflectors (unpublished).
[35] V. F. Nesterenko, *Dynamics of Heterogeneous Materials* (Springer-Verlag, New York, 2001).
[36] S. Ulrich, N. Upadhyaya, B. V. Opheusden, and V. Vitelli, Shear shocks in fragile networks, Proc. Natl. Acad. Sci. USA **110**, 20929 (2013).
[37] S. J. Orfanidis, *Electromagnetic Waves and Antennas* (Rutgers University Press, New Brunswick, NJ, 2002).
[38] S. Noda, M. Fujita, and T. Asano, Spontaneous-emission control by photonic crystals and nanocavities, Nat. Photon. **1**, 449 (2007).
[39] L. Onsager, Statistical hydrodynamics, Nuovo Cimento **6**, 279 (1949).
[40] M. Wilkinson, V. Bezuglyy, and B. Mehlig, Emergent order in rheoscopic swirls, J. Fluid Mech. **667**, 158 (2011).
[41] D. J. Griffiths, *Introduction to Electrodynamics*, 3rd ed. (Prentice Hall, Upper Saddle River, NJ, 1999).
[42] M. Born and E. Wolf, *Principles of Optics*, 4th ed. (Pergamon Press, New York, 1970).
[43] H. Furstenberg and H. Kesten, Products of random matrices, Ann. Math. Stat. **31**, 457 (1960).
[44] A. A. Abrikosov, The paradox with the static conductivity of a one dimensional metal, Solid State Commun. **37**, 997 (1981).
[45] http://spectrumthinfilms.com/stf/coatings/metallic-coatings-reflective/